A STRUCTURE-PRESERVING NUMERICAL DISCRETIZATION OF REVERSIBLE DIFFUSIONS

JUAN C. LATORRE*, PHILIPP METZNER †, CARSTEN HARTMANN ‡, AND CHRISTOF SCHÜTTE§

Abstract. We propose a robust and efficient numerical discretization scheme for the infinitesimal generator of a diffusion process based on a finite volume approximation. The resulting discrete-space operator can be interpreted as a jump process on the mesh whose invariant measure is precisely the cell approximation of the Boltzmann distribution of the original process. Moreover the resulting jump process preserves the detailed balance property of the original stochastic process.

Key words. Reversible diffusions, finite-volume method, detailed balance, coarse-graining.

1. Introduction and overview

In many applications, e.g., molecular dynamics [34], reaction kinetics [14] or systems biology [1] one is interested in discrete-state approximations of the following class of stochastic differential equations (SDE)

$$dX_t = -\nabla V(X_t)\,dt + \sqrt{2\beta^{-1}}dW_t\,, \quad X_0 = x\,. \tag{1.1}$$

Here W_t denotes standard Brownian motion on the state space of X_t, the function V is a smooth potential, and $\beta = 1/(k_B T)$ denotes inverse temperature with k_B being Boltzmann's constant (more precise statements are given below).

It is desirable that the numerical approximation of the stochastic process inherits some of the basic properties of the original equation such as its *stationary distribution* or *reversibility)*. The latter is equivalent to the requirement that the discretized process satisfies detailed balance which essentially asserts that the probability fluxes between equilibrium states are balanced [13]; therefore so any sensible discretization method for the problem at hand should be targeted on approximating the corresponding fluxes (this excludes, e.g., finite differences or finite elements approximations).

A method that is popular in computational fluid dynamics is the finite volume method as it is based on evaluating fluxes through the surfaces of the discretization volumes [38]. Moreover the method is conservative in the sense that the flux entering a certain volume is equal to the flux coming from the neighbouring volume [22]. The flux conservation property entails that there is no loss of probability at the boundaries of the computational domains; see also the related work [6] or [2] for a discussion of the Discontinuous Galerkin method. Moreover it turns out, as we will see later on in the numerical examples, that the method is efficient in that it is robust even when the discretization is very coarse.

In this paper we follow ideas of Wang, Peskin and Elston in [37] where a detailed balance preserving numerical algorithm is developed for the study of Brownian motors.

*To whom correspondence should be addressed: Freie Universität Berlin, Institut für Mathematik, Arnimallee 6, 14195 Berlin, Germany (latorre@mi.fu-berlin.de)

†Freie Universität Berlin, Institut für Mathematik, Arnimallee 6, 14195 Berlin, Germany (metzner@mi.fu-berlin.de)

‡Freie Universität Berlin, Institut für Mathematik, Arnimallee 6, 14195 Berlin, Germany (chartman@mi.fu-berlin.de)

§Freie Universität Berlin, Institut für Mathematik, Arnimallee 6, 14195 Berlin, Germany (schuette@mi.fu-berlin.de)

We present a numerical approximation of the second-order differential operator

$$\mathcal{L} = \beta^{-1}\Delta - \nabla V(x)\cdot\nabla \tag{1.2}$$

that is associated with the diffusion process (1.1) and that generates the semigroup $\exp(t\mathcal{L})$ of its solutions. We emphasize that our approach is inspired by the recent works [20, 19] in which the authors study Dirichlet problems of the form $\mathcal{L}f = q$ for the computation of mean exit times in the low temperature regime (cf. Section 3.3). Here we are rather interested in studying time-dependent problems associated with the SDE (1.1). One such problem is the backward Kolmogorov equation

$$\left(\frac{\partial}{\partial t} - \mathcal{L}\right) u(x,t) = 0, \quad u(x,0) = f(x). \tag{1.3}$$

To be precise, we want to solve the Cauchy problem (1.3) for $(x,t) \in \Omega \times [0,T]$ with $T < \infty$ and $\Omega \subset \mathbb{R}^n$ being a compact domain. As for the potential energy V we assume $V \in C^\infty(\Omega)$, bounded below and satisfying the usual growth conditions at infinity (in case when $|\Omega|$ grows large). The solution $u(x,t) = \exp(t\mathcal{L})f(x)$ can be expressed in terms of the diffusion (1.1) as follows:

$$u(x,t) = \mathbb{E}[f(X_t)|X_0 = x].$$

In other words, u is the average value of f evaluated along the characteristics X_t. Conversely, we may ask what is the probability distribution

$$\rho(x,t)dx = \mathbb{P}[X_t \in [x, x+dx)]$$

of X_t given that X_0 follows an initial distribution ρ_0. The probability density function $\rho(x,t)$ is then governed by the forward Kolmogorov or Fokker-Planck equation

$$\left(\frac{\partial}{\partial t} - \mathcal{L}^*\right) \rho(x,t) = 0, \quad \rho(x,0) = \rho_0(x) \tag{1.4}$$

which is the second problem that is studies in this article. Here $\mathcal{L}^*$ is the formal L^2 adjoint of $\mathcal{L}$, namely,

$$\mathcal{L}^* = \beta^{-1}\Delta + \nabla V(x)\cdot\nabla + \Delta V(x).$$

There are now several requirements that the discretization of $\mathcal{L}$ or $\mathcal{L}^*$ should fulfill:

1. The spatial discretization of the Boltzmann distribution

$$d\mu(x) = Z^{-1}e^{-\beta V(x)}dx, \quad Z = \int_\Omega e^{-\beta V(x)}\,dx \tag{1.5}$$

that is the stationary distribution of (1.1) should equal the stationary solution of the discretized Fokker-Planck equation (1.4). In particular, given a uniform discretization $x_1, x_2, \ldots, x_M$ of Ω, we require $\boldsymbol{\pi} = (\pi_1, \ldots, \pi_M)$ with $\pi_i = \exp(-\beta V(x_i))$ to be the stationary solution of (1.4), upon discretization and up to a normalization factor.
2. The discretization should preserve the forward backward dichotomy, i.e., when $\boldsymbol{A}$ denotes the spatial discretization of the infinitesimal generator $\mathcal{L}$, then we want $\boldsymbol{A}^T$ to be the discretization of its adjoint $\mathcal{L}^*$ (including boundary conditions).

3. Being related with the latter, we require that the discretization preserves detailed balance. That is, for all $(x,y)\in\Omega$ and $t\in[0,T]$ the transition probabilities satisfy

$$\mathbb{P}[X_t\in[x,x+dx)|X_0=y]d\mu(y)=\mathbb{P}[X_t\in[y,y+dy)|X_0=x]d\mu(x)$$

which implies that the time-reversed process $\tilde{X}_t=X_{T-t}$ with stationary initial condition $X_0\sim\mu$ follows the same SDE as the original process, hence has the same infinitesimal generator (cf. [13, 16]).

The article is organized as follows: in Section 2 we derive the structure-preserving finite volume discretization of the infinitesimal generator that gives rise to discretizations of the forward equation (Sec. 2.1) and the backward equation (Sec. 2.2). Section 3 contains a couple of numerical examples, both time-dependent and time-independent. We conclude by a brief discussion of the results in Section 4.

2. Finite volume approximation of the infinitesimal generator

In this section we derive a spatial discretization of the SDE (1.1) based on a finite volume approximation [21, 22] of backward and forward Kolmogorov equations. To this end, it is convenient to recast the infinitesimal generator (1.2) as

$$\mathcal{L}u=\beta^{-1}e^{\beta V}\nabla\cdot\left(e^{-\beta V}\nabla u\right), \tag{2.1}$$

and its adjoint as

$$\mathcal{L}^*\rho=\beta^{-1}\nabla\cdot\left(e^{-\beta V}\nabla\left(e^{\beta V}\rho\right)\right). \tag{2.2}$$

Now given a set of discretization points $\{x_i\}_{i=1}^M\subset\Omega$, we associate a finite volume element Ω_i to each point $x_i\in\Omega_i$ and introduce

$$p_i(t)=\int_{\Omega_i}\rho(x,t)\,dx$$

as the homogeneous probability distribution of X_t on the cell Ω_i. As we will show, the function $\boldsymbol{p}=(p_1,\ldots,p_M)^T$, $p_i=p_i(t)$ satisfies a discrete-state forward Kolmogorov (master) equation for a jump process on the mesh. Conversely the spatial discretization of the backward equation (1.3) results in a point-wise approximation of the function $u(x,t)$ at the mesh points x_i, i,.e.,

$$\boldsymbol{u}=(u_1,\ldots,u_M)^T,\quad u_i=u(x_i,t).$$

Use of symbols and standing assumptions. Before we derive the discretizations of forward and backward equation, we shall fix some notation that we will use in the following. We call (see Figure 2.1)

- $x_i\in\Omega$: mesh point i, $i=1,\ldots,M$; the discrete state space is denoted by S.
- Ω_i: finite volume element (cell) of mesh point $i\in S$,
- $m(A)$: Lebesgue measure (volume) of element $\boldsymbol{A}$,
- for every $i\in S$, we denote by $\{i_l\}$, $l=1,\ldots,M_i$ the subsequence, such that the $\{x_{i_l}\}$ are neighbours (adjacent mesh points) of x_i,
- $S_{i,j}$: boundary (plane segment) between Ω_i and Ω_j for $j\in\{i_l\}$,
- $h_{i,j}$: line segment connecting x_i and x_j for $j\in\{i_l\}$,
- $\bar{x}_{i,j}$: $S_{i,j}\cap h_{i,j}$ for $j\in\{i_l\}$.

We assume throughout that the cell elements Ω_i are rectangular. Accordingly, any vector $h_{i,j}$ connecting two neighbouring points x_i and x_j is perpendicular to the surface element $S_{i,j}$ dividing the neighbouring cells. Note, however, that this does not imply that the mesh is uniform along the principal coordinate directions.

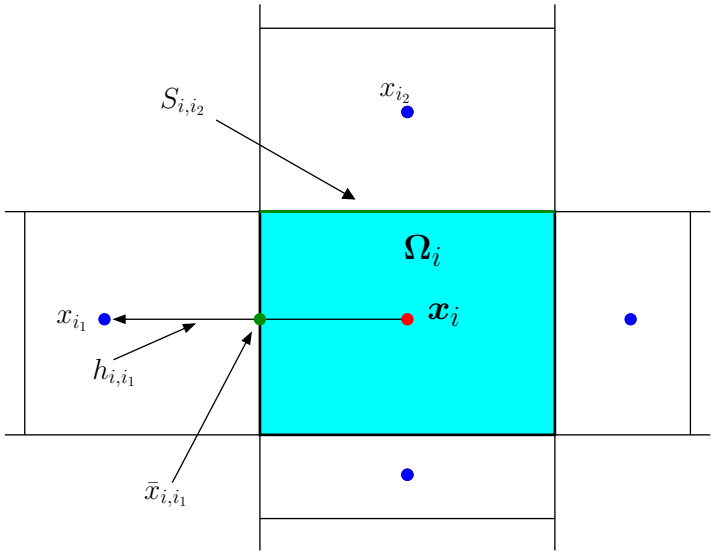

FIGURE 2.1. *Finite-volume element* Ω_i.

2.1. Numerical discretization of the forward equation

We firstly confine our attention to the forward Kolmogorov (Fokker-Planck) equation. To this end we use (2.2) and rewrite the forward equation (1.4) as

$$\frac{\partial}{\partial t}\rho(x,t) = \beta^{-1}\nabla\cdot\left(e^{-\beta V(x)}\nabla\left(e^{\beta V(x)}\rho(x,t)\right)\right).$$

Recalling that

$$p_i(t) = \int_{\Omega_i}\rho(x,t)\,dx$$

and using the divergence theorem it follows that

$$\begin{aligned}\frac{d}{dt}p_i(t) &= \int_{\Omega_i}\beta^{-1}\nabla\cdot\left(e^{-\beta V(x)}\nabla\left(e^{\beta V(x)}\rho\right)\right)dx\\ &= \sum_{l=1}^{M_i}\int_{S_{i,i_l}}\beta^{-1}e^{-\beta V(x)}\nabla\left(e^{\beta V(x)}\rho\right)\cdot\boldsymbol{n}\,ds.\end{aligned} \tag{2.3}$$

For all $j\in\{i_l\}$, we approximate each surface integral above as a point evaluation of the integrand at the middle point $\bar{x}_{i,j}$ times the area of $S_{i,j}$,

$$\begin{aligned}&\int_{S_{i,j}}\beta^{-1}e^{-\beta V(x)}\nabla\left(e^{\beta V(x)}\rho\right)\cdot\boldsymbol{n}ds\\ &\quad\approx\beta^{-1}e^{-\beta V(\bar{x}_{i,j})}\nabla\left(e^{\beta V(x)\rho}\right)\cdot\boldsymbol{n}\Big|_{x=\bar{x}_{i,j}}m(S_{i,j}).\end{aligned} \tag{2.4}$$

As we assume that the vector $h_{i,j}$ is parallel to the unit normal $\boldsymbol{n}$ to the surface $S_{i,j}$ diving the cells Ω_i and Ω_j, we can write

$$\nabla f\cdot\boldsymbol{n}\Big|_{x=\bar{x}_{i,j}} = \frac{\nabla f\cdot h_{i,j}}{m(h_{i,j})}\Big|_{x=\bar{x}_{i,j}},\quad j\in\{i_l\} \tag{2.5}$$

for any differentiable function f where $m(h_{i,j})$ here is just the length of the line $h_{i,j}$. But the last expression is simply directional derivative of f at $\bar{x}_{i,j}$. Hence, using a two-sided finite difference approximation between the points x_i and x_j, we obtain

$$\nabla\left(e^{\beta V(x)}\rho\right)\cdot\boldsymbol{n}\Big|_{x=\bar{x}_{i,j}} \approx \frac{e^{\beta V_j}\rho(x_j,t)-e^{\beta V_i}\rho(x_i,t)}{m(h_{i,j})}$$

where for simplicity we have used the shorthand $V_k = V(x_k)$. Upon employing the approximation

$$\int_{\Omega_i}\rho(x_i,t)\,dx \approx \rho(x_i,t)m(\Omega_i)$$

the probability flux on $S_{i,j}$ can be recast as

$$\begin{aligned}\int_{S_{i,j}} &\beta^{-1}e^{-\beta V(x)}\nabla\left(e^{\beta V(x)}\rho\right)\cdot\boldsymbol{n}ds \\ &\approx \frac{e^{-\beta(V_{i,j}-V_j)}}{\Delta_{j,i}}p_j(t) - \frac{e^{-\beta(V_{i,j}-V_i)}}{\Delta_{i,j}}p_i(t), \quad j\in\{i_l\},\end{aligned}$$

where

$$\frac{1}{\Delta_{i,j}} = \frac{\beta^{-1}m(S_{i,j})}{m(h_{i,j})m(\Omega_i)}, \quad j\in\{i_l\}.$$

Regrouping terms in (2.3), the approximation of (1.4) finally becomes

$$\frac{d}{dt}p_i(t) = \sum_{j\in\{i_l\}}\frac{e^{-\beta(V_{i,j}-V_j)}}{\Delta_{j,i}}p_j(t) - \left(\sum_{j\in\{i_l\}}^{M_i}\frac{e^{-\beta(V_{i,j}-V_i)}}{\Delta_{i,j}}\right)p_i(t) \tag{2.6}$$

or, in matrix vector notation,

$$\dot{\boldsymbol{p}}(t) = \boldsymbol{A}^T\boldsymbol{p}(t) \tag{2.7}$$

with $\boldsymbol{p}=(p_1,\ldots,p_M)^T$. Here and in the following dotted quantities such as $\dot{\boldsymbol{p}}=d\boldsymbol{p}/dt$ denote time derivatives and the elements of the matrix $\boldsymbol{A}\in\mathbb{R}^{M\times M}$ are given by

$$A_{i,j} = \begin{cases}\Delta_{i,j}^{-1}e^{-\beta(V_{i,j}-V_i)}, & j\in\{i_l\},\\ -\sum_{l=1}^{M_i}A_{i,i_l}, & j=i,\\ 0, & \text{otherwise.}\end{cases} \tag{2.8}$$

The matrix $\boldsymbol{A}$ has row sum zero and off-diagonal entries that are non-negative. Hence it has all properties of a generator matrix. In more specific terms, $\boldsymbol{A}$ is the infinitesimal generator of a jump process on the grid $\{x_i\}$ with the $A_{i,j}$ for $i\neq j$ being the jump rates between the discrete states x_i and x_j.

2.2. Finite-volume approximation of the backward equation

Next, we derive the finite volume approximation of the backward Kolmogorov equation (1.3) following the same ideas as for the forward case. It turns out that the resulting discretization of the infinitesimal generator $\mathcal{L}$ is precisely the discrete operator $\boldsymbol{A}$ from the previous section; note that this is not generally the case for any given spatial discretization method (e.g., finite differences).

Using the representation (2.1) of the generator $\mathcal{L}$ we proceed as before and recast the backward Kolmogorov equation as

$$\frac{\partial}{\partial t}u(x,t)=\beta^{-1}e^{\beta V(x)}\nabla\cdot\left(e^{-\beta V(x)}\nabla u(x,t)\right). \tag{2.9}$$

Setting $u_i(t)=u(x_i,t)$ and integrating (2.9) over the cell element Ω_i, we find

$$\begin{aligned}\frac{d}{dt}u_i(t)m(\Omega_i)&\approx\int_{\Omega_i}\beta^{-1}e^{\beta V(x)}\nabla\cdot\left(e^{-\beta V(x)}\nabla u\right)\\&\approx\beta^{-1}e^{\beta V(x_i)}\nabla\cdot\left(e^{-\beta V(x)}\nabla u\right)\Big|_{x=x_i}m(\Omega_i)\end{aligned}$$

where in the first equality we have made the approximation

$$\frac{d}{dt}u_i(t)m(\Omega_i)\approx\frac{d}{dt}\int_{\Omega_i}u(x,t)dx$$

and we have again approximated the volume integral as a point evaluation at $x=x_i$ times the volume of Ω_i. Doing a backward substitution, the divergence term in the above equation can be rewritten as

$$\begin{aligned}\nabla\cdot\left(e^{-\beta V(x)}\nabla u\right)\Big|_{x=x_i}m(\Omega_i)&\approx\int_{\Omega_i}\nabla\cdot\left(e^{-\beta V(x)}\nabla u\right)dx\\&=\sum_{j\in\{i_l\}}\int_{S_{i,j}}e^{-\beta V(x)}\nabla u\cdot\boldsymbol{n}ds.\end{aligned} \tag{2.10}$$

where the second line follows again from the divergence term. For each individual surface integral over $S_{i,j}$, $j\in\{i_l\}$ we may then write

$$\begin{aligned}\int_{S_{i,j}}e^{-\beta V(x)}\nabla u\cdot\boldsymbol{n}ds&\approx e^{-\beta V(x)}\nabla u\cdot\boldsymbol{n}\Big|_{x=\bar{x}_{i,j}}m(S_{i,j})\\&=e^{-\beta V_{i,j}}\frac{\nabla u\cdot h_{i,j}}{m(h_{i,j})}\Big|_{x=\bar{x}_{i,j}}m(S_{i,j})\\&\approx e^{-\beta V_{i,j}}\frac{u(x_j,\cdot)-u(x_i,\cdot)}{m(h_{i,j})}m(S_{i,j})\\&=\frac{e^{-\beta V_{i,j}}m(S_{i,j})}{m(h_{i,j})}u_j-\frac{e^{-\beta V_{i,j}}m(S_{i,j})}{m(h_{i,j})}u_i.\end{aligned}$$

As we did for the forward Kolmogorov equation, the surface integral has been approximated as a point evaluation of the integrand at $x=\bar{x}_{i,j}$, while the resulting normal derivative was replaced by a centered difference at the points $x=x_i$ and $x=x_j$. After regrouping terms in (2.10), we obtain

$$\begin{aligned}\frac{d}{dt}u_i(t)&=\sum_{j\in\{i_l\}}\frac{e^{-\beta(V_{i,j}^{-}-V_i)}}{\Delta_{i,j}}u_j(t)-\sum_{j\in\{i_l\}}\frac{e^{-\beta(V_{i,j}^{-}-V_i)}}{\Delta_{i,j}}u_i(t)\\&=\sum_{j\in\{i_l\}}A_{i,j}u_j(t)-\left(\sum_{j\in\{i_l\}}A_{i,j}\right)u_i(t)\end{aligned}$$

or, in matrix vector notation,

$$\dot{\boldsymbol{u}}(t) = \boldsymbol{A}\boldsymbol{u}(t), \tag{2.11}$$

where $A_{i,j}$ is precisely given by (2.8) thus proving that the finite volume approximation (FVA) of the backward Kolmogorov equation results in the adjoint equation of the forward Kolmogorov (master) equation (2.7) for the discrete-state system.

2.3. Properties of the semi-discretized Kolmogorov equations

1. Recall that the Boltzmann distribution

$$\mu(dx) = Z^{-1} e^{-\beta V(x)}\, dx, \quad Z = \int_\Omega e^{-\beta V(x)}\, dx$$

is the unique invariant distribution of the continuous state space process (1.1). On the other hand the homogeneous probability distribution of the process on the discretized state space S reads

$$\begin{aligned}\mathbb{P}[X \in \Omega_i] &= \int_{\Omega_i} d\mu(x) \\ &\approx Z^{-1} e^{-\beta V_i} m(\Omega_i).\end{aligned}$$

It can be readily seen that the vector

$$\boldsymbol{\pi} = (\pi_1, \ldots, \pi_M), \quad \pi_i \propto e^{-\beta V_i} m(\Omega_i). \tag{2.12}$$

is indeed a solution to the stationary Fokker-Planck equation for the discrete-state system, i.e., $\boldsymbol{A}^T\boldsymbol{\pi} = 0$. To see this, we substitute $\boldsymbol{\pi}$ into (2.6):

$$\begin{aligned}[\boldsymbol{A}^T\boldsymbol{\pi}]_i &= \sum_{l=1}^{M_i} \frac{e^{-\beta(V_{i,i_l} - V_{i_l})}}{\Delta_{i_l,i}} e^{-\beta V_{i_l}} m(\Omega_{i_l}) - \left(\sum_{l=1}^{M_i} \frac{e^{-\beta(V_{i,i_l} - V_i)}}{\Delta_{i,i_l}} \right) e^{-\beta V_i} m(\Omega_i) \\ &= \sum_{l=1}^{M_i} \frac{e^{-\beta(V_{i,i_l})}}{\Delta_{i_l,i}} m(\Omega_{i_l}) - \left(\sum_{l=1}^{M_i} \frac{e^{-\beta(V_{i,i_l})}}{\Delta_{i,i_l}} \right) m(\Omega_i) \\ &= \sum_{l=1}^{M_i} \frac{\beta^{-1} m(S_{i,i_l})}{m(h_{i_l,i})} e^{-\beta(V_{i,i_l})} - \left(\sum_{l=1}^{M_i} \frac{\beta^{-1} m(S_{i,i_l})}{m(h_{i,i_l})} e^{-\beta(V_{i,i_l})} \right) \\ &= 0\end{aligned}$$

where we have used $\bar{x}_{i,j} = \bar{x}_{j,i}$, $m(S_{i,j}) = m(S_{j,i})$ and $m(h_{i,j}) = m(h_{j,i})$, $j \in \{i_l\}$. Hence (2.12) is a stationary distribution of (2.7). In particular, the restriction of $\exp(-\beta V)$ to the grid points is a stationary distribution if the grid is uniform.

2. It is a straight consequence of (2.7) and (2.11) that the diagram

$$\begin{array}{ccc} \partial_t u = \mathcal{L} u & \xrightarrow{\text{adjoint in } L^2} & \partial_t \rho = \mathcal{L}^* \rho \\ \text{FVA}\big\downarrow & & \big\downarrow\text{FVA} \\ \dot{\boldsymbol{u}} = \boldsymbol{A}\boldsymbol{u} & \xrightarrow{\text{adjoint in } \mathbb{R}^n} & \dot{\boldsymbol{p}} = \boldsymbol{A}^T\boldsymbol{p}. \end{array}$$

commutes. Hence the finite volume approximation (FVA) yields adjointness of the discrete backward and forward equations.

3. Last but not least, the discretization preserves detailed balance, i.e., reversibility of the original process (i.e., X_t and X_{T-t} have the same generator). For a jump process with infinitesimal generator $\boldsymbol{A}$, the detailed balance condition reads

$$A_{i,j}\pi_i = A_{j,i}\pi_j \quad \forall i,j \in S.$$

For our jump process with master equation (2.6) the last equation holds true since $A_{i,j} = A_{j,i} = 0$ for $j \notin \{i_l\}$ which immediately implies $A_{i,j}\pi_i = A_{j,i}\pi_j$; for $j \in \{i_l\}$, we have

$$\begin{aligned}\pi_i A_{i,j} =& e^{-\beta V_i} m(\Omega_i) \frac{e^{-\beta(V_{i,i_l} - V_i)}}{\Delta_{i,i_l}} \\ =& \frac{\beta^{-1} m(S_{i,i_l})}{m(h_{i,i_l})} e^{-\beta V_{i,i_l}},\end{aligned}$$

while

$$\begin{aligned}\pi_j A_{j,i} =& e^{-\beta V_{i_l}} m(\Omega_{i_l}) \frac{e^{-\beta(V_{i_l,i} - V_{i_l})}}{\Delta_{i_l,i}} \\ =& \frac{\beta^{-1} m(S_{i,i_l})}{m(h_{i,i_l})} e^{-\beta V_{i,i_l}}\end{aligned}$$

which proves the assertion that the discrete system is again reversible.

2.4. On the accuracy of the method and non-rectangular grids

Before we conclude with the discretization section we would like to briefly elaborate on error estimates for our finite volume approximation as well as commenting on the assumptions underlying the definition of the cell elements.

Assuming a uniform mesh, every cell has the same length h in each spatial-direction. Hence the finite volume approximation of the special backward generator (2.1) is equivalent to using centered finite differences at each mesh point x_i. To be more precise, for the divergence term in (2.1), one can use a centered finite difference between the points $x_{i+1/2}$ and $x_{i-1/2}$ (for each coordinate direction in Ω), resulting in the evaluation of the potential at the "mid-points" $\bar{x}_{i_l}$. The gradient ∇u at $\bar{x}_{i_l}$ can then be approximated again by a centered finite difference between the points x_i and $x_{i\pm1}$. This will result in the discrete state approximation (2.8) of the infinitesimal generator $\mathcal{L}$. Given these simplifying assumptions and assuming some regularity of the potential V, the finite volume discretization (2.8) turns out to be a consistent approximation of the infinitesimal generator (1.2) that is second-order accurate [7, 35, 22]. This assertion will be verified numerically in Section 3.2 when we show the solution of Dirichlet problems of the type $\mathcal{L}f = q$. In [37] where a similar numerical scheme is considered, it is argued that the numerical algorithm is robust even for potentials that may have discontinuities.

In the derivation of the numerical algorithm we have assumed that the cell elements are n-dimensional hyperrectangles and that, along each direction, the neighbouring points of each mesh point are connected by a vector normal to the cell dividing surfaces. In principle, the hypothesis that each cell element must be rectangular can be relaxed; in fact each cell element may have any arbitrary convex polygonal shape without affecting the overall method — probably even without affecting reversibility or the forward-backward dichotomy. But we could no longer approximate the

probability flux along each boundary as in (2.4) simply using finite differences; as a consequence the scheme would not admit an expression for the discrete generator as simple as (2.8), but rather require the computation of certain surface integrals which may be tedious if the problem becomes high-dimensional (cf. also [3] and the references therein). There are clearly other methods to approximate fluxes in a finite volume setting (see e.g. [11]), but these may not result in the desired form of the infinitesimal generator.

3. Numerical Experiments

In this section we illustrate the finite volume approximation (FVA) with several test problems. Especially we will show that our numerical method is robust, even for a relatively coarse box discretization. This particular aspect is demonstrated in detail in our first example. The second example is concerned with solving mixed-boundary value problems involving the backward generator $\mathcal{L}$. Finally in the last example, we apply the FVA to rare events problems and study the rearrangement of a three-particle Lennard-Jones cluster in the plane.

3.1. Sampling the invariant distribution

The first numerical demonstration will be to sample the invariant distribution of a low dimensional potential landscape and to compare it to a standard Monte-Carlo scheme.

3.1.1. Sampling from MJP

To sample the stationary distribution of the SDE (1.1) we exploit the characterization of the matrix $\boldsymbol{A}$ as the infinitesimal generator of a Markov jump process (MJP) on the discrete state space S which i) is a discrete analog of the original process and ii) preserves reversibility with respect to the approximated Boltzmann measure. The idea now is to draw a realization from the MJP, i.e., a sequence $(i_1,t_{i_1};i_2,t_{i_2};\ldots;i_N,t_{i_N})$ of states $i_k\in S$ and residence times t_{i_k} that the process spends in the state i_k before jumping to the next state i_{k+1}. Generating a realization of a MJP with generator $\boldsymbol{A}$ can be performed by the following iteration [29]: Suppose the MJP starts in $i_0\in S$. Then

1. draw a resident time t_{i_k} according to
$$t_{i_k}=\log(u)(A_{i_k,i_k})^{-1}$$
with u uniformly distributed on $[0,1]$,
2. draw the next state i_{k+1} with probability
$$\mathbb{P}[i_{k+1}=j]\propto A_{i_k,j}\quad j\neq i_k.$$

3.1.2. Convergence to the invariant measure

Now we may ask how fast does our scheme sample the invariant measure and how does it perform compared to a standard integrator like Euler-Maruyama. Suppose that at time $t=0$ the MJP is distributed according to the initial probability distribution $\boldsymbol{\nu}$. Further let $\boldsymbol{p}(t)$ be the distribution at time $t\geq 0$ that is governed by the *master equation* [5],

$$\frac{d\boldsymbol{p}(t)}{dt}=\mathbf{A}^T\boldsymbol{p}(t),\quad \boldsymbol{p}(0)=\boldsymbol{\nu}.$$

By construction, the invariant measure of our MJP $\boldsymbol{\pi}$ solves $\boldsymbol{A}^T\boldsymbol{\pi}=0$. Given a uniform grid on Ω the vector $\boldsymbol{\pi}$ has the elements

$$\pi_i=Z^{-1}\exp(-\beta V(x_i)),\quad i\in S,$$

with Z^{-1} being the normalization constant and x_i being the center of cell Ω_i. Reversibility implies that the MJP converges exponentially to its invariant measure. More precisely, let $0=\lambda_1>\lambda_2\geq\lambda_3\geq\ldots\geq\lambda_{|S|}$ be the eigenvalues of $\mathbf{A}$. By reversibility, all eigenvalues are real and the following estimate holds [27, 28]:

$$\|\boldsymbol{p}(t)-\boldsymbol{\pi}\|_1\leq K\,e^{\lambda_2 t},\quad t\geq 0$$

where $\|\cdot\|_1$ is the discrete l_1-norm and $K>0$ is a constant depending on $\mathbf{A}$.

Conversely for SDEs of the type (1.1) applying the Euler-Maruyama scheme (see, e.g., [18]) yields an time-discrete iteration of the form

$$\hat{X}_{k+1}=\hat{X}_k-\nabla V(\hat{X}_k)\tau+\sqrt{2\beta^{-1}\tau}\,\eta \tag{3.1}$$

where $\hat{X}_k$ denotes the time-discrete approximation of X_{t_k} with $\hat{X}_0=X_0$, $\tau=t_{k+1}-t_k$ is the integration time step, and η is a $\mathcal{N}(0,1)$ Gaussian random variable.

For a general, multi-well potential V, sampling the Boltzmann distribution using (3.1) requires exponentially long trajectories. Therefore the time discretization inevitably introduces a bias in the invariant distribution of the SDE, even as $\tau\to 0$. Even worse, if the gradient field ∇V is nonglobally Lipschitz then the Euler-Maruyama scheme is transient for all $\tau>0$ with unbounded moments [23]. The bias can be removed by augmenting the iteration (3.1) with an additional Metropolis-Hastings acceptance step, thereby using the Euler iteration merely as a proposal generator for a Monte-Carlo sampler [32, 4]. Using an approximation to the true dynamics for generating proposals rather than completely random moves guarantees that the proposals are "physically sensible" and the rejection rate is low. Moreover the scheme converges with probability one to the correct Boltzmann distribution for any stable step size $\tau>0$.

3.1.3. On how to compare MJP with Euler-Maruyama

Comparing a MJP with the Euler-based Monte-Carlo scheme sounds like comparing apples and oranges, for Euler-Maruyama is a *time discretization* method, whereas our approach is based on a *spatial discretization* of the infinitesimal generator. In addition, Euler-Maruyama scheme is stochastic in a continuous state space, whereas the MJP is stochastic in a discrete state space and stochastic in time. In the first case, moreover, the state space is unbounded. Hence, for a comparison of both schemes, the process is restricted to a bounded domain $\Omega\subset\mathbb{R}^n$ (here: $n=2$) where *restriction* means that Ω is chosen such the probability to find the equilibrated process in regions close to the boundary of Ω is of the order of the machine accuracy.

Now let $S=\{\Omega_1,\ldots,\Omega_{M^2}\}$ be a grid (box discretization) covering the domain $\Omega\subset\mathbb{R}^2$ with M^2 equal sized boxes. The invariant distribution of the SDE restricted on the boxes is then given by the discrete Boltzmann distribution

$$\hat{\boldsymbol{\pi}}=(\hat{\pi}_1,\ldots,\hat{\pi}_{M^2}),\quad \hat{\pi}_i=Z^{-1}\int_{\Omega_i}\exp(-\beta V(x,y))dxdy,$$

with Z being a normalization constant. Although the exact stationary distribution of the corresponding MJP is different, namely,

$$\boldsymbol{\pi}=(\pi_1,\ldots,\pi_{M^2}),\quad \pi_i\propto\exp(-\beta V(x_i,y_{j_i}))$$

we may still compare the MJP and the Euler-Maruyama scheme in terms of their convergence to $\hat{\boldsymbol{\pi}}$, for the difference between $\boldsymbol{\pi}$ and $\hat{\boldsymbol{\pi}}$ is negligible.

We measure the convergence of either method by the l_1-norm,

$$\mathbb{E}[\|\hat{\boldsymbol{\pi}} - \tilde{\boldsymbol{p}}(T)\|_1], \tag{3.2}$$

where $\tilde{\boldsymbol{p}}(T) = (\tilde{p}_1(T), \ldots, \tilde{p}_{M^2}(T))$ denotes the state probability distribution resulting from a finite realization of the MJP or the Euler-Maruyama scheme at time $T > 0$. To be more precise, the state probability distribution, $\tilde{\boldsymbol{p}}(T)$, associated with a realization of the MJP, $(i_0, t_{i_0}; \ldots; i_N, t_{i_N} = T)$, is computed by the time average

$$\hat{p}_j(T) = \frac{1}{T} \sum_{k=0}^{N} t_{i_k} \delta_{j,i_k} \quad \forall j \in S,$$

whereas the distribution of the Metropolis-adjusted Euler scheme is computed from a normalized histogram whose bins are defined by the cells Ω_i.

In order to make the convergence results of both methods comparable, the simulations are coupled such that they require the same total numerical effort. To understand the following algorithmic procedure it is helpful to bear in mind that we are interested in computing expectations values. Therefore we generate an *ensemble* consisting of $L > 0$ trajectories with a total time $T > 0$ from either method and approximate the expectation value by averaging over the different realizations. Furthermore it is important to realize that the number of jumps N of a MJP-trajectories of total time $T > 0$ is *random* and, hence, the total numerical effort of generating L trajectories,

$$C_{MJP} = \sum_{i=1}^{L} N_i, \tag{3.3}$$

is random too. Consequently, choosing $N_{Euler} = C_{MJP}/L$ and $\tau = T/N_{Euler}$ in the Metropolis-adjusted Euler-Maruyama scheme leads to the same total numerical effort as for the MJP scheme. The numerical experiment is summarized as follows:

1. For a fixed total time $T > 0$, generate $L > 0$ MJP-trajectories.
2. Approximate the expectation in (3.2) by running averages of $\|\hat{\boldsymbol{\pi}} - \tilde{\boldsymbol{p}}(T)\|_1$.
3. Generate $L > 0$ trajectories with the Metropolis-Euler-Maruyama scheme of constant length $N_{Euler} = C_{MJP}/L$ and constant time step $\tau = T/N_{Euler}$.
4. Approximate the expectation in (3.2) by running averages.

3.1.4. Numerical results

As a potential in (1.1) we choose the 2-dimensional three-well potential

$$\begin{aligned} V(x,y) = & 3e^{-x^2-\left(y-\frac{1}{3}\right)^2} - 3e^{-x^2-\left(y-\frac{5}{3}\right)^2} \\ & - 5e^{-(x-1)^2-y^2} - 5e^{-(x+1)^2-y^2} + \tfrac{1}{5}x^4 + \tfrac{1}{5}\left(y-\tfrac{1}{3}\right)^4 \end{aligned} \tag{3.4}$$

that is a well-known test example for studying rare events (see, e.g., [17, 30, 26]). As the left panel of Figure 3.1 shows, the potential (3.4) has two deep minima approximately at $(\pm 1, 0)$, a shallow minimum approximately at $(0, 1.5)$, three saddle points approximately at $(\pm 0.6, 1.1), (-1.4, 0)$ and a maximum at $(0, 0.5)$.

For the inverse temperature $\beta = 1.67$, the invariant distribution $\mu \propto \exp(-\beta V)$ is shown in the right panel of Figure 3.1. The sharp peaks located at the minima of the potential indicate that the dynamics (1.1) are metastable, i.e., the process spends a long time in the vicinity of a minimum before it makes a transition to another well.

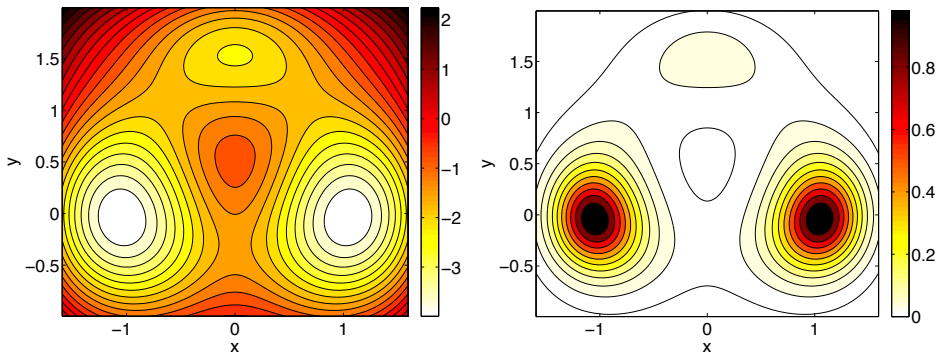

FIGURE 3.1. *Left panel: Contour plot of the three-well potential in (3.4). Right panel: The invariant distribution,* $\exp(-\beta V)$*, of the Markov process in (1.1) for the inverse temperature* $\beta = 1.67$ *indicates metastability.*

In other words, the process exhibits a slow time scale which prevents the process from fast equilibrating which implies slow convergence of any sampling procedure.

The convergence of the schemes is compared using three differently sized grids, $M = 20, 40, 60$, each covering the same rectangular domain $\Omega = [-2,2] \times [-1.5, 2.5]$; for a detailed description of the numerical experiment see the previous section. The discrete Boltzmann distribution is sufficiently accurately computed on these grids by using quadrature. The expected numerical error in (3.2) is approximated by an average, $\langle \|\hat{\boldsymbol{\pi}} - \hat{\boldsymbol{p}}(T)\|_1 \rangle$, computed from $L = 1000$ realizations where each realization starts in the same state, namely, in the center of the cell covering the point $(-1, 0)$ being the center of the left minimum.

The average l_1-error as a function of the total time $T = 10000, 20000, \ldots, 100000$ is illustrated in the panels of Figure 3.2. As one can see, the convergence of the methods considerably differs on the coarsest grid (see left panel). The double logarithmic plot reveals geometric convergence of the Metropolised Euler-Maruyama scheme with rate $1/2$, but the MJP converges at a slower rate. Even worse, the average $\langle \|\hat{\boldsymbol{\pi}} - \tilde{\boldsymbol{p}}(T)\|_1 \rangle$ seems to be bounded from below by a constant. Explaining this behaviour is simple: the lower bound (as indicated by the dashed line) is the error $\|\boldsymbol{\pi} - \hat{\boldsymbol{\pi}}\|_1$. The graph particularly shows that the observable $\tilde{\boldsymbol{p}}(T)$ is almost converged at the final time $T = 100000$. The plots in the middle and in the right panel reveal that the convergence on a finer but still coarse grid ($M = 40, 60$) is comparable with the convergence of the Metropolis-adjusted Euler-Maruyama scheme (which is also reversible).

Next we turn our attention to the first non-trivial eigenvalue, $\lambda_2 < 0$, of the generator matrix $\boldsymbol{A}$ as a function of the total number of discretization boxes. The eigenvalue λ_2 indicates the slowest time scale the MJP which, here, is the transition process between the two metastable regions in the three-well potential (cf. Fig. 3.1).[1] As one can see in Figure 3.3, the eigenvalue λ_2 quickly converges as the number of the boxes increases ($M = 20, 40, 60, \ldots, 300$). Particularly, the graph shows that even for a coarse discretization, e.g., $M = 40$, the essential dynamics of the SDE, i.e., the hopping between the two major metastable sets is well captured by the MJP.

[1] Notice that the numerical computation of the eigenvalues and vectors of the generator matrix $\boldsymbol{A}$ is well-conditioned since $\boldsymbol{A}$ is algebraically similar to a symmetric matrix, $\mathrm{diag}(\boldsymbol{\pi}^{1/2})\,\boldsymbol{A}\,\mathrm{diag}(\boldsymbol{\pi}^{-1/2})$

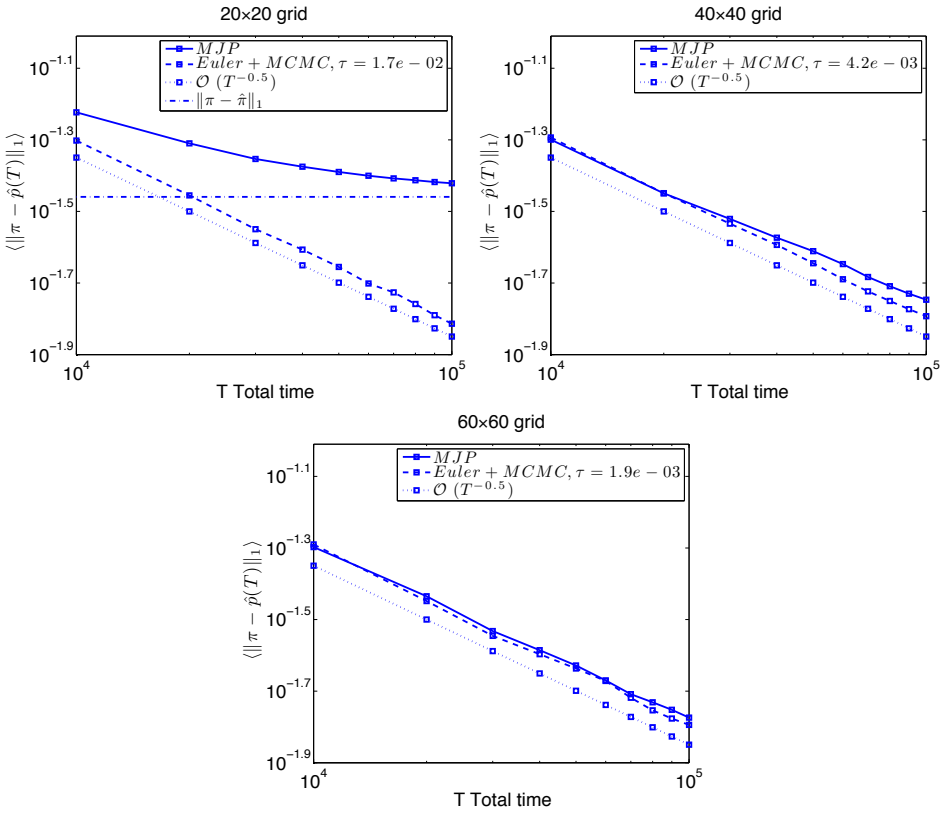

FIGURE 3.2. *Convergence of the schemes with respect to the discrete Boltzmann distribution* $\hat{\boldsymbol{\pi}}$ *is illustrated by the average* l_1*-error as a function of the total time* $T=10000,20000,\cdots,100000$. *The MJP (solid line) is compared to Metropolis-Euler-Maruyama scheme (dashed lines) using three differently sized grids with* $M=20,40,60$.

3.2. Committor for the two-well potential

We now test our numerical algorithm for solving *mixed boundary value problems* of the type

$$\begin{cases} \mathcal{L}q=0 & \text{in } \Omega, \\ q=0 & \text{on } \partial A, \\ q=1 & \text{on } \partial B, \\ \nabla q\cdot\boldsymbol{n}=0 & \text{on } \partial\Omega, \end{cases} \tag{3.5}$$

where $\mathcal{L}$ is the backward generator given in (1.2), $\Omega\subset\mathbb{R}^n$ is a compact set with smooth boundary $\partial\Omega$, the sets $A,B\subset\Omega$ are two open, disjoined subsets with smooth boundaries $\partial A,\partial B$, and $\boldsymbol{n}$ denotes the outward pointing unit normal to $\partial\Omega$. The function q solving (3.5) is referred to as the *forward committor function* and plays an important role in the analysis of rare events of Markov processes, in particular in *Transition Path Theory* (TPT); we shall come back to TPT type problems in Sect. 3.3.

with $\boldsymbol{\pi}$ being the stationary distribution of the MJP.

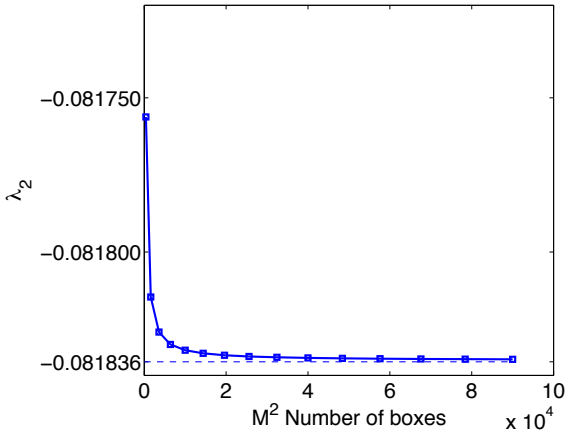

FIGURE 3.3. *The graph shows the first nontrivial eigenvalue, $\lambda_2 < 0$, of the generator matrix $\boldsymbol{A}$ (defined in (2.8) as a function of the total number of discretization boxes. The quick convergences indicates that the MJP even for a coarse grid well captures the essential dynamics of the underlying SDE. Results for $M = 20, 40, \ldots, 300$ and $\beta = 1.67$.*

In our numerical experiment, we consider a two-well potential in two dimensions,

$$V(x,y) = \frac{5}{2}\left(1-x^2\right) + 5y^2, \tag{3.6}$$

on a rectangular domain $\Omega = [-1,1] \times [-0.8, 0.8]$. The contour plot of the potential landscape is given in the left panel of Figure 3.4. If the sets A and B are chosen as

$$A = \{(x,y) : x < -0.8\} \cap \Omega \text{ and } B = \{(x,y) : x > 0.8\} \cap \Omega$$

then the committor equation in (3.5) admits the analytical solution [10]

$$q(x,y) = \left(\int_{-0.8}^{0.8} e^{\frac{5}{2}(1-z^2)^2} dz) \right)^{-1} \int_{-0.8}^{x} e^{\frac{5}{2}(1-z^2)^2} dz \tag{3.7}$$

that is shown in the right panel of Figure 3.4. Notice that the exact committor function only depends on the coordinate x (because the sets A and B do) and it can be sufficiently accurately computed using quadrature.

The exact committor function allows for numerically computing the order of accuracy of our scheme that is expected to be of second order. To this end the committor equation is numerically solved with the finite volume scheme on a sequence of grids on $\Omega_{A,B}$where each grid consists of M^2 equal sized boxes (cells) for $M = 20, \ldots, 200$ and covers the set $\Omega \setminus (A \cup B)$. The numerical error $\|q - \hat{q}\|_\infty$ between the exact committor function q evaluated at the box centers and the numerical solution $\hat{q}$ is depicted in Figure 3.5 as a function of the box width (here: in the x-direction, h_x). The double logarithmic plot reveals the second order accuracy of our scheme. Additionally, the committor equation is numerically solved with standard finite differences schemes [15] on the grid spanned by the box centers of the grid. In particular, the finite volume scheme is compared to a central differences scheme (resulting from a second order discretization of the gradient term in $\mathcal{L}$ via central differences) and an upwind scheme (resulting from a first order upwind discretization of $\mathcal{L}$). It can be seen that the finite volume scheme clearly beats the finite differences schemes.

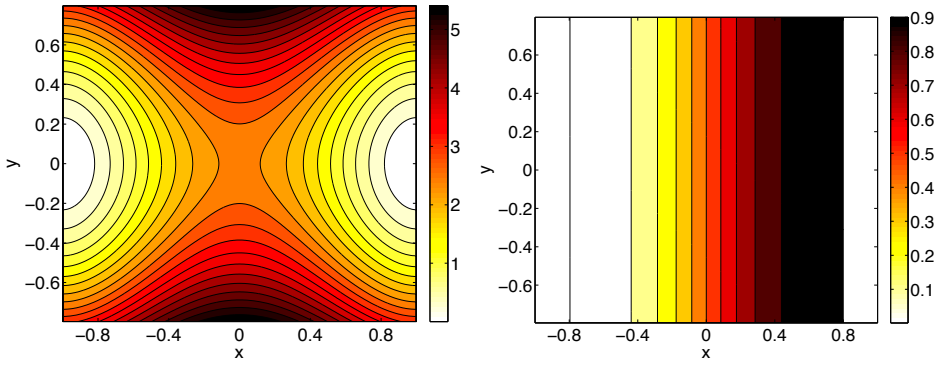

FIGURE 3.4. *Left panel: The contour plot of the two-well potential given in (3.6) on the domain* $\Omega = [-1,1] \times [-0.8,0.8]$. *Right panel: The level sets of the exact committor function* $q(x,y)$ *given in (3.7) for the inverse temperature* $\beta = 1$. *The value* $q(x,y)$ *admits a probabilistic interpretation; it is the probability that the process starting in* (x,y) *reach the set* $A = \{(x,y) : x < -0.8\} \cap \Omega$ *first rather than the set* $B = \{(x,y) : x > 0.8\} \cap \Omega$.

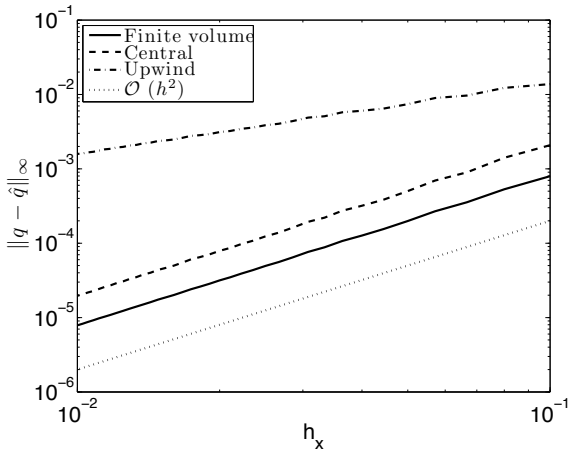

FIGURE 3.5. *Numerical error* $\|q - \hat{q}\|_\infty$ *between the exact committor function* q *and the numerical solution* $\hat{q}$ *of the committor equation (3.5) as a function of the spatial discretization in* x*-direction,* h_x.

3.3. Application to Lennard-Jones cluster rearrangement

In the first example we have shown that the FVA, interpreted as a MJP, properly captures the essential dynamics of the diffusion process (1.1), given a coarse discretization of the computational domain. The purpose of the last example is to demonstrate that the FVA can be even applied to identify *rare events*, i.e., transitions between metastable regions. More specifically, we demonstrate the interplay between our discretization scheme and discrete Transition Path Theory, a recently introduced method to deal with rare events in Markov jump processes.

3.3.1. Transition Path Theory

Transition Path Theory (TPT) is concerned with transitions in Markov processes

and has first been developed in [10, 36, 25] in the context of diffusion processes, in particular for systems of the form in (1.1). The basic idea is to single out two disjoint subsets in state space, say, $A,B\subset\Omega$ and determine the "preferred" mechanism by which the dynamics makes a transition (reaction) from A to B. Typically the sets A and B are metastable regions representing, e.g., conformations of biomolecules [33]. Transitions between metastable regions are rare events and therefore any sampling-based method for the detection of transitions mechanisms and transition rates would cause an enormous numerical effort.

TPT goes beyond sampling in that the underlying committor function completely encodes the statistical properties of the ensemble of all reactive trajectories (transitions) can be efficiently computed by solving a mixed boundary value problem in (3.5). TPT provides expressions for the probability distribution of reactive trajectories, the associated probability current and flux, and the corresponding transition rates. In applications one is often interested in identifying the most probable transition mechanism from A to B, i.e, in the region in state space through which the most transitions happen per unit of time. Accordingly the transition tubes are characterized by the current of reactive trajectories. Accurately solving the PDE (3.5) is of course impossible if the problem's dimensions is high. The remedy then is *discrete TPT - Transition Path Theory for Markov jump processes* that is a generalization of TPT to the Markov jump processes [26]. Within the discrete TPT framework the reactive properties of a system are captured in a discrete transition network and the preferred transition pathways can effectively computed via Graph algorithms [24].

3.3.2. Lennard-Jones cluster

Inspired by the considerations in [8, 39], we are take a look at the rearrangement of a cluster of three particles in the plane whose dynamics is governed by the Smoluchowski dynamics (1.1). The interaction of the particles is described by the Lennard-Jones potential

$$V_{LJ}(\mathbf{x}^1,\mathbf{x}^2,\mathbf{x}^3)=\sum_{1\le i<j\le 3}4\epsilon\left[\left(\frac{\sigma}{|\ \mathbf{x}^i-\mathbf{x}^j|}\right)^{12}-\left(\frac{\sigma}{|\ \mathbf{x}^i-\mathbf{x}^j|}\right)^{6}\right],\tag{3.8}$$

where $\mathbf{x}^i\in\mathbb{R}^2,\ i=1,2,3$ denotes the position of i-th particle. The potential assumes its minimum at

$$(\mathbf{m}^1,\mathbf{m}^2,\mathbf{m}^3)\in\left\{(\mathbf{x}^1,\mathbf{x}^2,\mathbf{x}^3):\|\ \mathbf{x}^i-\mathbf{x}^j\|_2=2^{1/6}\sigma,\ 1\le i<j\le 3\right\}$$

with $V(\mathbf{m}^1,\mathbf{m}^2,\mathbf{m}^3)=-3\epsilon$. Geometrically this minimizer corresponds to a triangular arrangement of the three particles with constant distance $r_{min}=2^{1/6}\sigma$. Although the potential is invariant under translation and rotation, we assume that the particles are distinguishable. Therefore there are two essentially different equilibrium configurations as is schematically illustrated in Figure 3.6. In the following we refer to the left configuration in the figure as $1-2-3$ and to the right one as $1-3-2$.

The question now is the following: what is the preferred rearrangement of the cluster starting in the $1-2-3$ configuration and ending up in the $1-3-2$ one and how does the preferred transition path changes as temperature is varied?

Formulated in the language of discrete TPT, we ask what is the *dominant reaction pathway* from $1-2-3$ (set A) to $1-3-2$ (set B)? A cheap way of going from state A to state B would be clearly by rotating the whole molecule. In order to exclude this possibility we break the symmetry by i) fixing particle one in the origin and ii)

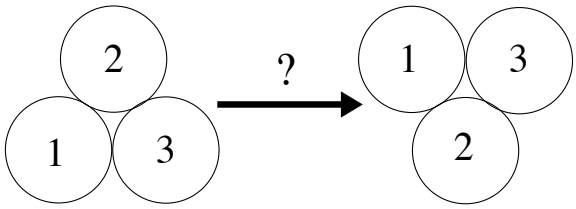

FIGURE 3.6. *Schematic illustration of the two different equilibrated configurations of the three particle Lennard-Jones cluster in the plane. The interaction of the particle is described by the potential in (3.8). We are interested in the rearrangement of the left configuration (denoted by* $1-2-3$*) to the right configuration (denoted by* $1-3-2$*) under the Smoluchowski dynamics.*

restricting the movement of particle three to the x-axis of the plane. The dynamics of the restricted cluster are then governed by a three-dimensional potential landscape of the form

$$V(x_1^2,x_2^2,x_1^3) \stackrel{def}{=} V_{LJ}\left((0,0),(x_1^2,x_2^2),(x_1^3,0)\right).$$

The corresponding MJP as a discrete analog of (1.1) results from a coarse $30\times30\times30$ box discretization of the rectangular domain $\Omega=[0,r_{cut}]\times[-r_{cut},r_{cut}]\times[0,r_{cut}]$ with $r_{cut}=2.5\sigma\approx2.22\cdot10^{-1}$. For the well-depth $\epsilon=5$, the configurations $1-2-3$ and $1-3-2$ are metastable configurations. To ensure that the MJP is irreducible — at least for all practical purposes — only boxes with a potential energy below a prescribed threshold are considered. In other words, grid points with too high potential energy (compared to the minimum -3ϵ) are negligible as their invariant measure is vanishingly small and henceforth omitted.

In principle only two different transition mechanisms are possible for the transition from the $1-2-3$ to the $1-3-2$ configuration; either particle two moves down on a vertical straight line while particle three is sidestepping, or particle three remains fixed while particle two is circumventing. Notice that the symmetric case, i.e., circumventing particle one, is excluded by the choice of Ω. The computation of the dominant reaction pathway via discrete TPT shows that at high temperature, $\beta=1$, the first mechanism is preferred, whereas at low temperature, $\beta=5$, the second one is preferred. For a schematic illustration of the pathways see Figure 3.7. From a physical point of view this behaviour is reasonable as the path through the "middle" is admissible, only if particle three is far away enough from particle one, so that particle two can slip through. At high temperature this scenario is relatively probable, for particle three moves rapidly back and forth and there is a "finite window" for particle two to slip through However the window becomes smaller and smaller the lower temperature gets. Therefore the dynamics prefers the circumventing route at low temperature since it is not conditioned by the position of particle number three.

A mathematical argument for the validity of the explanation is given by the theory of Freidlin and Wentzell [12] which states that at low temperature the dynamics prefers the transition pathways along the lowest energy barriers; the potential energies of the two respective dominant reaction paths is depicted in Figure 3.7. As indicated by the dashed lines, the highest barrier at low temperature (left panel) is indeed less than the one at high temperature (right panel). Besides the preferred reaction pathway, discrete TPT gives us the transition rate k_{AB}, i.e., the average number of transitions from A to B per unit of time. Note that at low temperature, $\beta=5$, the transition

rate is $k_{AB}=2.9\cdot10^{-8}$; for such a small k_{AB}, any attempt to detect the transition behaviour by sampling of (1.1) would inevitably fail.

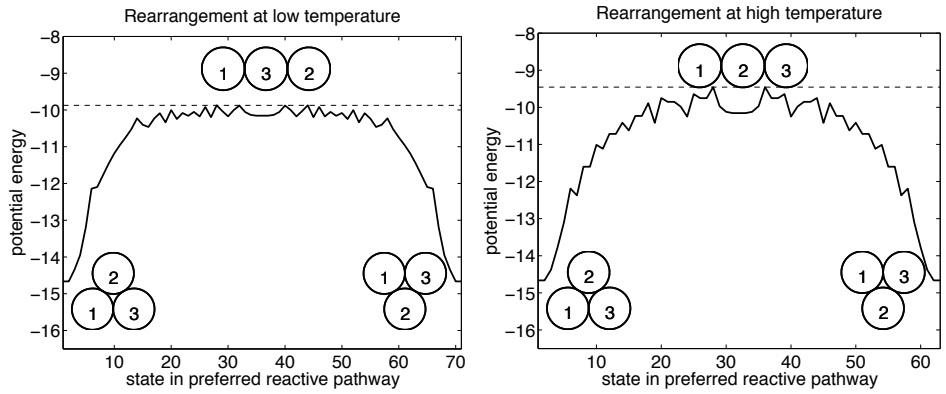

FIGURE 3.7. *Potential energy along the reaction pathway from the initial cluster configuration* $1-2-3$ *to the final cluster configuration* $1-3-2$. *Left panel: Energy profile for the low temperature* $\beta=5$. *Right panel: Energy profile for the high temperature* $\beta=1$. *Results are shown for* $\epsilon=5$ *and a* $30\times30\times30$ *box discretization of the rectangular domain* $\Omega=[0,r_{cut}]\times[-r_{cut},r_{cut}]\times[0,r_{cut}]$ *with* $r_{cut}=2.5\sigma\approx2.22\cdot10^{-1}$.

4. Conclusion and outlook

In this paper we have developed a numerical algorithm based on a finite volume discretization of the infinitesimal generator $\mathcal{L}$ of stochastic differential equations of Smoluchowski type. The resulting discretized operator, $\boldsymbol{A}$, can be interpreted as the infinitesimal generator (rate matrix) of a Markov jump process (MJP) on the chosen grid. By simulating the jump process one can then generate trajectories on the discretized state space (as supposed to discrete-time trajectories as in standard numerical discretization of SDEs). We have shown that our numerical method preserves important properties associated with the original continuous process such as the invariant measure, the forward-backward dichotomy and detailed balance (reversibility), independently of the grid size. Since the discretization preserves detailed balance, the eigenvalues of the discretized infinitesimal generator remain real-valued.

We have also shown with some simple numerical examples that our discretization is suitable for solving boundary value problems as they arise in Transition Path Theory for, e.g., detecting transition mechanisms in molecules, even given only a coarse discretization. Moreover we have demonstrated that the discrete MJP provides an (ergodic) sampling scheme that allows for computing the discretized Boltzmann distribution without bias, further being exponentially convergent with a rate that is comparable to a Metropolis-adjusted Euler-Maruyama scheme.

There are some issues that arise from any space discretization that we should mention: When the dimension of state space is too large, a spatial discretization is infeasible, although our method is robust for rather coarse meshes. We are currently investigating the possibility of directly computing coarse-grained generator matrices when the system exhibits temporal or spatial scale separation, in which case the averaging principle or homogenization theory applies. The corresponding effective coefficients such as free energy, Fixman potential or effective diffusivity (see [31]) can then be recovered consistently from the continuous state process and it is plausible

that they can be estimated from short simulations of the high dimensional system. Such an approach is much in the spirit of heterogeneous multiscale methods [9] and will be addressed in a forthcoming article.

A further extension of the finite volume scheme that we mention here only for completeness, is the formulation of the method on unstructured meshes, e.g., Delaunay triangulation involving an orthogonality condition. In order to avoid the combinatorial explosion in the number of cells in higher dimensions this implies that one needs to derive a priori error estimates as indicated in [3] to allow for adaptive mesh refinement. Eventually, being independent of specific grid geometries, would make the method applicable to real world problems such as conformation dynamics of biomolecules.

Acknowledgement. We would like to thank Ralf Kornhuber for valuable discussions about finite volume geometries and for pointing out useful references. This work is supported by the DFG Research Center MATHEON "Mathematics for Key Technologies" (FZT86) in Berlin.

REFERENCES

[1] D.H. Anderson. *Compartmental Modeling and Tracer Kinetics*, volume 50 of *Lecture Notes in Biomathematics*. Springer, Berlin, 1983.
[2] D.N. Arnold, F. Brezzi, B. Cockburn, and L.D. Marini. Unified analysis of discontinuous galerkin methods for elliptic problems. *SIAM J. Numer. Anal.*, 39(5):1749–1779, 2002.
[3] R. E. Bank, W. M. Coughran, Jr., and L. C. Cowsar. The finite volume Scharfetter-Gummel method for steady convection diffusion equations. *Comput. Vis. Sci.*, 1(3):123–136, 1998.
[4] N. Bou-Rabee and E. Vanden-Eijnden. Pathwise accuracy and ergodicity of metropolized integrators for sdes. *Comm. Pure Appl. Math.*, 63(5):655–696, 2010.
[5] P. Brémaud. *Markov Chains: Gibbs Fields, Monte Carlo Simulation and Queues*. Springer Verlag, 1999.
[6] F. Brezzi, L. D. Marini, and P. Pietra. Two-dimensional exponential fitting and applications to drift-diffusion models. *SIAM J. Numer. Anal.*, 26(6):1342–1355, 1989.
[7] Z. Cai, J. Mandel, and S. McCormick. The finite volume element method for diffusion equations on general triangulations. *SIAM J. Numer. Anal.*, 28(2):392–402, 1991.
[8] C. Dellago, P. Bolhuis, and D. Chandler. Efficient transition path sampling: Applications to lennard-jones cluster rearrangements. *J. Chem. Phys.*, 108(22):9236–9245, 2098.
[9] W. E, B. Engquist, X. Li, W. Ren, and E. Vanden-Eijnden. Heterogeneous multiscale methods: A review. *Comm. Comput. Phys.*, 2(3):367–450, 2007.
[10] W. E and E. Vanden-Eijnden. Towards a theory of transition paths. *J. Statist. Phys.*, 123(3):503–523, 2006.
[11] C. Erath and D. Praetorius. A posteriori error estimate and adaptive mesh-refinement for the cell-centered finite volume method for elliptic boundary value problems. *SIAM J. Numer. Anal.*, 47(1):109–135, 2008.
[12] M.I. Freidlin and A.D. Wentzell. *Random Perturbations of Dynamical Systems*. Springer, New York, 1984.
[13] C.W. Gardiner. *Handbook of Stachastic Methods: For Physics, Chemistry and the Natural Sciences*. Springer, 2nd edition, 1996.
[14] D.T. Gillespie. A general method for numerically simulating the stochastic time evolution of coupled chemical reactions. *J. Comput. Phys.*, 22(4):403–434, 1976.
[15] W. Hackbusch. *Elliptic differential Equations: Theory and numerical treatment*. Springer-Verlag, 1992.
[16] U. G. Haussmann and E. Pardoux. Time reversal of diffusions. *Ann. Probab.*, 14(4):1188–1205, 1986.
[17] S. Huo and J. E. Straub. The maxflux algorithm for calculating variationally optimized reaction paths for conformational transitions in many body systems at finite temperature. *J. Chem. Phys.*, 107(13):5000–5006, 1997.
[18] Peter E. Kloeden and Eckhard. Platen. *Numerical solution of stochastic differential equations*. Springer-Verlag, 1992.
[19] P. R. Kramer, J. C. Latorre, and A. A. Khan. Two coarse-graining studies of stochastic models in molecular biology. *Commun. Math. Sci.*, 8(2):482–517, 2010.

[20] J. C. Latorre. *Effective Transport Properties of Stochastic Biophysical Models*. Doctoral thesis, Rensselaer Polytechnic Intitute, 2008.
[21] R.J. LeVeque. *Numerical Methods for Conservations Laws*. Birkhäuser, Bassel, 1990.
[22] R.J. LeVeque. *Finite Volume Methods for Hyperbolic Problems*. Cambridge University Press, 2002.
[23] J. C. Mattingly, A. M. Stuart, and D. J. Higham. Ergodicity for SDEs and approximations: locally Lipschitz vector fields and degenerate noise. *Stoch. Proc. Appl.*, 101(2):185–232, 2002.
[24] P. Metzner. *Transition path theory for Markov processes*. PhD thesis, Freie Universität Berlin, 2007.
[25] P. Metzner, Ch. Schütte, and E. Vanden-Eijnden. Illustration of transition path theory on a collection of simple examples. *J. Chem. Phys.*, 125(8):084110, 2006.
[26] P. Metzner, Ch. Schütte, and E. Vanden-Eijnden. Transition path theory for Markov jump processes. *Multiscale Model. Simul.*, 7(3):1192–1219, 2009.
[27] S.P. Meyn and R.L. Tweedie. *Markov Chains and Stochastic Stability*. Springer, London, 1993.
[28] A. Yu. Mitrophanov. Stability and exponential convergence of continuous-time markov chains. *J. Appl. Probab.*, 40(4):970–979, 2003.
[29] J. R. Norris. *Markov chains*. Cambridge University Press, 1998.
[30] S. Park, M. K. Sener, D. Lu, and K. Schulten. Reaction paths based on mean first-passage times. *J. Chem. Phys.*, 119(3):1313–1319, 2003.
[31] G.A. Pavliotis and A.M. Stuart. *Multiscale Methods: Averaging and Homogenization*. Springer, 2008.
[32] G.O. Roberts and R.L. Tweedie. Exponential convergence of langevin distributions and their discrete approximations. *Bernoulli*, 2(4):341–363, 1996.
[33] Ch. Schütte and W. Huisinga. Biomolecular conformations can be identified as metastable sets of molecular dynamics. In P. G. Ciarlet and C. Le Bris, editors, *Special Volume: Computational Chemistry*, volume X of *Handbook of Numerical Analysis*, pages 699–744. Elsevier, 2003.
[34] N. Singhal, C.D. Snow, and V.S. Pande. Using path sampling to build better Markovian state models: Predicting the folding rate and mechanism of a tryptophan zipper beta hairpin. *J. Chem. Phys.*, 121(1):415–425, 2004.
[35] J.W. Thomas. *Numerical Partial Differential Equations; Finite Difference Methods*. Springer, New York, 1995.
[36] E. Vanden-Eijnden. Transition path theory. In M. Ferrario, G. Ciccotti, and K. Binder, editors, *Computer Simulations in Condensed Matter: from Materials to Chemical Biology*, volume 2 of *703*. Springer Verlag, 2006.
[37] H. Wang, C. S. Peskin, and T. C. Elston. A robust numerical algorithm for studying biomolecular transport processes. *J. Theoret. Biol.*, 221(4):491–511, 2003.
[38] P. Wesseling. *Principles of Computational Fluid Dynamics*. Springer, Berlin, 2001.
[39] T. Yanao, W. S. Koon, and J. E. Marsden. Mass-related dynamical barriers in triatomic reactions. *Few-Body Systems*, 38(2-4):161–166, 2006.